Int J Fract (2019) 217:49–64
https://doi.org/10.1007/s10704-019-00362-0

ORIGINAL PAPER

A super-convergent staggered algorithm for the simulation of hydraulic fracturing treatments

M. Vahab · **N. Khalili**

Received: 11 July 2018 / Accepted: 8 May 2019 / Published online: 21 May 2019

Abstract In this paper, a super-convergent algorithm is presented for the simulation of hydraulic fracturing process in impervious domains using the extended finite element framework. The hydro-fracture inflow is modeled based on the Darcy law, in which the fracture permeability is incorporated by taking advantages from the well-known cubic law. The hydro-mechanical coupling between the fracturing fluid flow and the surrounding bulk is carried out by employing a sequential iterative procedure known as the staggered Newton algorithm. The convergence rate of the existing staggered solutions in the literature is examined, and an alternative super-convergent approach is proposed. Finally, through several numerical simulations the sanity of the developed framework is demonstrated.

Keywords Hydraulic fracture propagation · Extended finite element method · Staggered Newton iteration · Convergence study

1 Introduction

Hydraulic fracturing treatment is a well-known engineering process during which highly conductive fractures are generated within low permeability formations due to highly pressurized fluid injection. Analytical solutions to the hydraulic fracturing problem are generally limited to the growth of a single hydro-fracture in an idealized homogeneous medium (e.g., Spence and Sharp 1985; Geertsma and De Klerk 1969; Desroches et al. 1994; Detournay 2004). On the contrary, numerical models are capable of tackling more complicated mechanisms encountered in practice including bulk inhomogeneities, multi-stage multizone treatments, gel leakage, and the presence of propping agent (e.g., Daneshy 1978; Beach 1980; Boone and Ingraffea 1990; Schrefler et al. 2006; Vahab and Khalili 2017, 2018). More recently, advanced computational frameworks such as X-FEM (e.g., Réthoré et al. 2007; Taleghani and Olson 2011; Khoei et al. 2014, 2015, 2016, 2018; Gordeliy and Peirce 2013, 2015), Meshless (e.g., Samimi and Pak 2016; Wang et al. 2010) and Phase-field (e.g., Lee et al. 2016, 2017; Wilson and Landis 2016; Xia et al. 2017) are employed in the simulation of hydraulic fracturing treatments in a computationally more efficient fashion.

In a wide range of engineering problems, different types of coupling may manifest due to the interaction of sources related to thermal, hydraulic, mechanical, chemical, electrical and magnetic actions. In the literature, two distinct computational strategies have been developed in order to tackle coupled systems, namely the monolithic (fully coupled) and the staggered (partitioned) schemes. The monolithic approaches take advantages from the direct solution of the complete system of coupled equations (Simoni and Schrefler 1991).

M. Vahab (✉) · N. Khalili
School of Civil and Environmental Engineering, UNSW Australia, Sydney 2052, Australia
e-mail: m.vahab@unsw.edu.au

The well-known ($\mathbf{u}-p$) formulation of the deformable porous media is probably amongst the most controversial formulation in this category, in which a unified unknown vector–including both the displacement ($\mathbf{u}$) and the pore fluid pressure (p) DOFs–is formed and solved simultaneously (Segura and Carol 2008). Alternatively, based on the staggered implementation, each field variable is solved individually while the rest of the subsystems are temporarily frozen at a predicted known value (Prevost 1997). Through the introduction of appropriate coupling components, each subsystem is solved and updated in a sequential manner until convergence is attained. The application of partitioned algorithms is well-understood in a variety of coupled problems, including the hydro-mechanical analysis (Prevost 1997; Zienkiewicz et al. 1988), the thermo-hydro-mechanical problem (Schrefler et al. 1997), and the fluid-structure interaction (Farhat and Lesoinne 2000; Matthies and Steindorf 2003).

The monolithic solution technique is proven to be highly consistent and rigorous in the solution of coupled systems (Lewis et al. 1991; Simoni and Schrefler 1991). However, several difficulties may arise due to the fact that: (i) it necessitates the development of new modules for the solution of each coupled system, and (ii) it leads to very large matrixes, particularly for 3D analysis, which may only be handled through sparse data storage (Prevost 1997; Saad 2003). On the contrary, the partitioned solutions are advantageous due to the: (i) modularity feature that enables distinct *specialized* modules to be linked in a modular fashion depending on the needs of the analysis, (ii) algorithmic structure, which facilitates parallel or sequential processing, and (iii) computational efficiency as it circumvents the requirement of the assembly and solution of the full system of coupled equations which is proven to be excessively costly (Prevost 1997). The staggered procedures, generally, on the contrary, bear difficulties in convergence, particularly in problems involving strong coupling (Segura and Carol 2008). Nonetheless, the enumerated prevailing features–despite the fact they are conditionally stable–have led to wide application of the partitioned solvers in the design of computational frameworks (e.g., Simoni and Schrefler 1991; Zienkiewicz and Chan 1989; Lewis et al. 1991; Boone and Ingraffea 1990; Khoei et al. 2015).

In the present study, a novel staggered Newton procedure is proposed for the hydro-mechanical coupling analysis of the fracking problem with a super-convergent rate. The hydro-fracture inflow is modeled by incorporating the cubic law, in which an aperture dependent permeability is assumed through the fracture. Meanwhile, the surrounding continuum is supposed to be impervious with no hydro-mechanical coupling. The existing staggered solutions for the hydraulic fracturing problem are challenged regarding their convergence rate and are compared against the proposed framework. The paper is organized as follows: in Sect. 2, the strong, weak and discrete formulation of the momentum balance of the bulk as well the fracturing fluid flow is presented. Section 3 is dedicated to the partitioned Newton solution procedure. In Sect. 4, the robustness of the proposed formulation is investigated. Finally, in Sect. 5 concluding remarks are illustrated.

2 Problem statement

Consider a 2D impervious domain Ω, bounded by the external boundary Γ, with the unit normal vector $\mathbf{n}_\Gamma$ as shown in Fig. 1a. The domain contains a hydro-fracture interface $\Gamma_{\mathcal{HF}}$ subjected to the incompressible Newtonian viscous fluid injection at the constant rate of $\mathcal{Q}_{\mathcal{INJ}}$. The external boundary is subjected to the prescribed traction $\mathbf{t}$ and the prescribed displacement $\bar{\mathbf{u}}$ which are respectively imposed on Γ_t and Γ_u, such that $\Gamma_t \cup \Gamma_u = \Gamma$ and $\Gamma_t \cap \Gamma_u = \varnothing$ hold. The hydro-fracture faces are indicated by positive and negative signs, with $\mathbf{n}_{\Gamma_{\mathcal{HF}}}$ being the normal unit vector exerted onto the negative side of $\Gamma_{\mathcal{HF}}$. The hydro-fracture faces may undergo fracturing fluid pressure p, while cohesive tractions $\mathbf{t}^{coh}$ are formed in the vicinity of the fracture tip to account for the nonlinearities associated with the stress field. In the following sections, the governing equations of the fractured bulk in conjunction with the hydro-fracture inflow are presented in detail.

2.1 Fractured bulk

The linear momentum balance equation governs the response of the fractured impervious domain. Using the infinitesimal deformation assumption, the momentum balance equation associated with the quasi-static condition is expressed as

$$\nabla \cdot \boldsymbol{\sigma} + \rho \mathbf{b} = \mathbf{0}. \tag{1}$$

In the above relation, $\mathbf{b}$ is the body force per unit mass vector, ρ denotes the bulk density, and $\boldsymbol{\sigma}$ stands for the

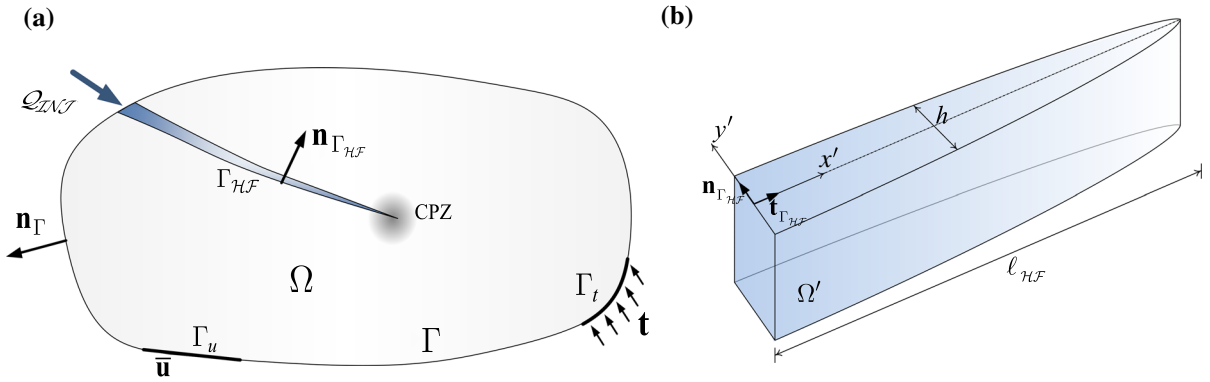

Fig. 1 Problem definition and boundary condition associated with, **a** the fractured domain containing a hydro-fracture interface; **b** the hydro-fracture inflow

Cauchy stress tensor. Note that the Cauchy stress tensor is related to the total strain tensor versus the constitutive relation $\boldsymbol{\sigma} = \mathbf{D} : \boldsymbol{\varepsilon}$, where $\mathbf{D}$ is the constitutive matrix (Hook's elasticity tensor in here), and $\boldsymbol{\varepsilon}$ is the strain tensor defined as $\boldsymbol{\varepsilon}(\mathbf{u}) = \nabla^s \mathbf{u}$. The external and internal boundary conditions corresponding to the fractured impervious domain are described as

$$\begin{aligned} &\textit{Internal Boundary Conditions} : \begin{cases} \boldsymbol{\sigma}\mathbf{n}_\Gamma = \mathbf{t} & \text{on } \Gamma_t, \\ \mathbf{u} = \bar{\mathbf{u}} & \text{on } \Gamma_u, \end{cases} \\ &\textit{External Boundary Conditions} : \boldsymbol{\sigma}\mathbf{n}_{\Gamma_{\mathcal{HF}}} \\ &\quad = p\mathbf{n}_{\Gamma_{\mathcal{HF}}} + \mathbf{t}^{cohs} \quad \text{on } \Gamma_{\mathcal{HF}}. \end{aligned} \tag{2}$$

where $\mathbf{n}$ denoting the unit normal vector, p being the fracturing fluid pressure, and $\mathbf{t}^{cohs}$ being the cohesive tractions. The weak formulation of the current boundary value problem is obtained through the introduction of the trail and test functions of the displacement field $\mathbf{u}(\boldsymbol{x}, t)$ and $\delta\mathbf{u}(\boldsymbol{x}, t)$, respectively. Notably, the test function $\delta\mathbf{u}(\boldsymbol{x}, t)$ must be adequately smooth to vanish on the essential boundary conditions, while the trial function $\mathbf{u}(\boldsymbol{x}, t)$ is required to meet the essential boundary conditions and to be smooth enough to define the essential derivatives. Following the standard procedure in derivation of the weak form, it yields

$$\begin{aligned} \delta\Pi^{bulk} = &\int_\Omega \delta\boldsymbol{\varepsilon} : \boldsymbol{\sigma} d\Omega + \int_{\Gamma_{\mathcal{HF}}} [\![\delta\mathbf{u}]\!] \cdot p\mathbf{n}_{\Gamma_{\mathcal{HF}}} d\Gamma \\ &+ \int_{\Gamma_{\mathcal{HF}}} [\![\delta\mathbf{u}]\!] \cdot \mathbf{t}^{cohs} d\Gamma - \int_\Omega \delta\mathbf{u} \cdot \rho\mathbf{b} d\Omega \\ &- \int_\Gamma \delta\mathbf{u} \cdot \mathbf{t} d\Gamma = 0. \end{aligned} \tag{3}$$

In the above relation, $[\![\delta\mathbf{u}]\!]$ denotes jump in the variational displacement vector $\delta\mathbf{u}$ across the fracture interface (i.e., $[\![\delta\mathbf{u}]\!] = \delta\mathbf{u}^+ - \delta\mathbf{u}^-$). Notably, the cohesive traction is a function of the jump in displacement field (i.e., $\mathbf{t}^{cohs} = \mathbf{t}^{cohs}([\![\mathbf{u}]\!])$), which is defined through constitutive relations known as traction-separation laws (Wells and Sluys 2001). In this study, a decaying exponential function is applied to capture the material softening behavior in the vicinity of the cohesive crack-tip zone as (Nguyen et al. 2001; Simoni and Schrefler 2014):

$$t_N^{\text{cohs}}(h) = \mathbf{t}^{cohs}(h).\mathbf{n}_{\Gamma_{\mathcal{HF}}} = \sigma_{\text{ult}} \exp(-\alpha h) \tag{4}$$

in which $\alpha = \sigma_{\text{ult}}/G_f$, with G_f and σ_{ult} denoting the fracture energy and the ultimate tensile strength of the domain, respectively. In addition, h is the crack opening defined as $h = [\![\mathbf{u}]\!].\mathbf{n}_{\Gamma_{\mathcal{HF}}} = [\![u_N]\!]$. Based on the cohesive zone model, cohesive crack tips evolve whenever the stress level exceeds beyond the ultimate tensile strength of the material.

Using the X-FEM, the discretized form of the displacement field is obtained by employing the shifted Heaviside enrichment function along the hydro-fracture interface $\Gamma_{\mathcal{HF}}$. Accordingly, the displacement field $\mathbf{u}^h(\boldsymbol{x}, t)$ is expressed by

$$\begin{aligned} \mathbf{u}^h(\boldsymbol{x}, t) &= \mathbf{N}(\boldsymbol{x})\mathbf{U}(t) + \tilde{\mathbf{N}}^{\mathcal{HF}}(\boldsymbol{x})\tilde{\mathbf{U}}^{\mathcal{HF}}(t) \\ &= \sum_{I\in\mathcal{N}} N_I(\boldsymbol{x})\mathbf{u}_I(t) + \sum_{I\in\mathcal{N}^{\mathcal{HF}}} N_I(\boldsymbol{x}). \\ &\quad [\mathcal{H}(\phi_{\Gamma_{\mathcal{HF}}}(\boldsymbol{x})) - \mathcal{H}(\phi_{\Gamma_{\mathcal{HF}}}(\boldsymbol{x}_I))]\tilde{\mathbf{u}}_I^{\mathcal{HF}}(t), \end{aligned} \tag{5}$$

where $\mathcal{N}$ and $\mathcal{N}^{\mathcal{HF}}$ are, respectively, the complete and enriched nodal sets associated with the standard and enriched DOFs of the displacement field $\mathbf{u}_I$ and $\tilde{\mathbf{u}}_I^{\mathcal{HF}}$. Moreover, N_I is the standard shape function associated with node I, and $\mathcal{H}$ is the Heaviside enrichment

function corresponding to the level set function $\phi_{\Gamma_{\mathcal{HF}}}$. Finally, $\mathbf{N}$ and $\tilde{\mathbf{N}}^{\mathcal{HF}}$ are, respectively, the matrix form of the standard and enriched shape functions associated with the standard and enriched vector of displacement DOFs $\mathbf{U}(t)$ and $\tilde{\mathbf{U}}^{\mathcal{HF}}(t)$. The matrix form of the equilibrium equation is acquired as

$$\begin{aligned}\boldsymbol{\Psi} &= \left\{\begin{array}{l}\boldsymbol{\Psi}_1\\ \boldsymbol{\Psi}_2\end{array}\right\}\\ &= \left\{\begin{array}{l}\mathbf{F}_{int}-\mathbf{F}_{ext}\\ \tilde{\mathbf{F}}^{\mathcal{HF}}_{int}-\tilde{\mathbf{F}}^{\mathcal{HF}}_{ext}+\mathcal{F}^{cohs}+\mathcal{F}^{\mathcal{HF}}\end{array}\right\}=0,\end{aligned} \tag{6}$$

where $\boldsymbol{\Psi}$ stands for the residual force vector in which

$$\begin{aligned}&\mathbf{F}_{ext}=\int_{\Gamma_t}\mathbf{N}^T\mathbf{t}d\Gamma+\int_{\Omega}\mathbf{N}^T\mathbf{b}d\Omega, && \mathbf{F}_{int}=\int_{\Omega}\mathbf{B}^T\boldsymbol{\sigma}d\Omega,\\ &\tilde{\mathbf{F}}^{\mathcal{HF}}_{ext}=\int_{\Gamma_{\mathcal{HF}}}(\tilde{\mathbf{N}}^{\mathcal{HF}})^T\mathbf{t}d\Gamma+\int_{\Omega}(\tilde{\mathbf{N}}^{\mathcal{HF}})^T\mathbf{b}d\Omega, && \tilde{\mathbf{F}}^{\mathcal{HF}}_{int}=\int_{\Omega}(\tilde{\mathbf{B}}^{\mathcal{HF}})^T\boldsymbol{\sigma}d\Omega,\\ &\mathcal{F}^{\mathcal{HF}}=\int_{\Gamma_{\mathcal{HF}}}\mathbf{N}^T p\mathbf{n}_{\Gamma_{\mathcal{HF}}}d\Gamma, && \mathcal{F}^{cohs}=\int_{\Gamma_{\mathcal{HF}}}\mathbf{N}^T\mathbf{t}^{cohs}d\Gamma.\end{aligned} \tag{7}$$

Note that in the above relations, the shape function derivatives are denoted by $\mathbf{B}(\boldsymbol{x})\equiv\mathbf{LN}(\boldsymbol{x})$ and $\mathbf{B}^{\mathcal{HF}}(\boldsymbol{x})\equiv\mathbf{L}\tilde{\mathbf{N}}^{\mathcal{HF}}(\boldsymbol{x})$, with $\mathbf{L}$ being the standard matrix of differential operators.

2.2 Hydro-fracture inflow

Consider a hydro-fracture interface in the local Cartesian coordinate system (x', y') as depicted in Fig. 1b. The hydro-fracture inflow is supposed to be incompressible, and one-dimensional with negligible width to length ratio. Neglecting the variations of the fracturing fluid pressure across the hydro-fracture section (i.e., $\partial p/\partial y'=0$), the continuity equation can be described as

$$\frac{\partial\mathcal{Q}}{\partial x'}+[\![\dot{u}_{\mathrm{N}}]\!]=0,\qquad 0\le x'\le\ell_{\mathcal{HF}} \tag{8}$$

where $\mathcal{Q}$ is the flow rate, $[\![u_{\mathrm{N}}]\!]$ is the projection of displacement field jump in direction normal to the interface (i.e., $[\![u_{\mathrm{N}}]\!]=[\![\mathbf{u}]\!].\mathbf{n}_{\Gamma_{\mathcal{HF}}}\equiv h$), and $\ell_{\mathcal{HF}}$ is the hydro-fracture length. In the above relation, the overdot indicates the derivative with respect to time. Note that the leak-off term can be added to Eq. (8) on the basis of a selection of approximate relations (e.g., Carter 1957).

The hydro-fracture inflow is modeled by taking advantages from the Darcy law as

$$\mathcal{Q}=\frac{1}{f}\frac{h^3}{12\mu}\frac{\partial p}{\partial x'}\equiv\frac{\kappa_{\mathcal{HF}}}{\mu}\frac{\partial p}{\partial x'}, \tag{9}$$

in which $\kappa_{\mathcal{HF}}$ is the hydro-fracture permeability determined on the basis of the cubic law ($\kappa_{\mathcal{HF}}=\kappa h$, where κ is the intrinsic permeability of the fracture), μ is the fluid dynamic viscosity, and f is the modification factor in range of 1.04–1.65 originally suggested by Witherspoon et al. (1980) to account for deviations from the ideal condition of smooth crack faces in laminar flow condition (for non-Darcian flow condition see Chen et al. 2019).

The boundary conditions associated with the hydro-fracture are determined based on the assumption of zero-lag between the flow front and the crack tip in conjunction with the flow rate at the injection point as

$$\mathcal{HF}\ \textit{Boundary Conditions}: \left\{\begin{array}{l}\mathcal{Q}|_{x'=0}=\mathcal{Q}_{\mathcal{INJ}},\\ \mathcal{Q}|_{x'=\ell_{\mathcal{HF}}}=0.\end{array}\right. \tag{10}$$

The finite difference method is utilized for the solution of the equations governing the hydro-fracture inflow. To this end, the discretization points are supposed to be a set of points positioned at the intersection of the hydro-fracture with the element edges. The fluid pressure p and flow rate $\mathcal{Q}$ along the hydro-fracture are approximated by adopting the first-order upwind scheme as

$$\begin{aligned}\frac{\partial\mathcal{Q}^{j+1}_n}{\partial x'_n}&=\frac{\mathcal{Q}^{j+1}_n-\mathcal{Q}^{j}_n}{\Delta x_n'^{j}},\\ \frac{\partial p^{j+1}_n}{\partial x'_n}&=\frac{p^{j+1}_n-p^{j}_n}{\Delta x_n'^{j}},\end{aligned} \tag{11}$$

where j stands for the jth discretization point, and n indicates the nth time step of the solution. In a similar manner, the crack opening velocity $[\![\dot{u}_{\mathrm{N}}]\!]$ is approximated by

$$[\![\dot{u}_{\mathrm{N}}]\!]^{j}_{n+1}=\frac{[\![u_{\mathrm{N}}]\!]^{j}_{n+1}-[\![u_{\mathrm{N}}]\!]^{j}_{n}}{\Delta t}. \tag{12}$$

in which Δt is the time increment adopted for the time domain discretization (i.e., $\Delta t=t_{n+1}-t_n$). It is noteworthy that positive values obtained for the fracturing fluid pressure are not added in this study due to the fact that no fluid may sustain suctions beyond its vapour

pressure p_v. Indeed, this phenomenon occurs as a result of delay in the flow front with respect to the fracture tip evolution, which is referred to as the *fluid-lag* in the literature (Mohammadnejad and Khoei 2013). Following Boone and Ingraffea (1990), the fracturing fluid pressure is capped at the vapour pressure in the current study.

3 Solution strategy

In this section, the staggered solution procedure employed for the coupled hydro-mechanical analysis is represented. Moreover, the fixed-point algorithm applied for the imposition of the boundary conditions to the hydro-fracture inflow is described.

3.1 The staggered Newton solution procedure

The staggered Newton scheme takes advantages from an iterative procedure which considers the solution of each set of the governing equations separately in a sequential manner. Accordingly, within each time step, the iterative procedure starts with the assumption of a fixed fracturing fluid pressure along the hydro-fracture interface, and it solves the solid phase equations. To this end, the momentum balance equation given by Eq. (6) is linearized using the standard Newton–Raphson procedure as

$$\boldsymbol{\Psi}_n^{i+1} = \boldsymbol{\Psi}_n^{i} + (\mathfrak{J}_{\mathbb{U}})_n^i \mathrm{d}\mathbb{U}_n^{i+1} = \mathbf{0}. \tag{13}$$

In the above relation, $\mathfrak{J}_{\mathbb{U}}$ is the tangential Jacobian matrix (stiffness matrix) given by $\mathfrak{J}_{\mathbb{U}} = \partial\boldsymbol{\Psi}/\partial\mathbb{U}$, in which $\mathbb{U} = \left\langle \mathbf{U}(t) \quad \tilde{\mathbf{U}}^{\mathcal{HF}}(t) \right\rangle$ is the complete set of displacement field DOFs, and i stands for the iteration number. The displacement field is then updated by $\mathbb{U}_n^{i+1} = \mathbb{U}_n^i + \mathrm{d}\mathbb{U}_n^i$, which in turn results in the updated fracture profile. Next, the updated displacement field is regarded as fixed, and the discrete form of the flow continuity in Eqs. (8–9) can be solved along the hydro-fracture as

$$\begin{cases} \mathbb{Q} = \mathfrak{J}_{\mathbb{Q}}^{i+1}\mathbb{H}, \\ \mathbb{P} = \mathfrak{J}_{\mathbb{P}}^{i+1}\mathbb{Q}, \end{cases} \tag{14}$$

where $\mathbb{Q}$, $\mathbb{P}$ and $\mathbb{H}$ are, respectively, the vectors containing the values of the flow rate, pressure and opening at discretization points, with $\mathfrak{J}_{\mathbb{Q}}$ and $\mathfrak{J}_{\mathbb{P}}$ being the matrix of coefficients manifested in a finite difference solution. The updated pressure field is adopted in order to start the next iteration. The iterative procedure is repeated until a convergence criterion is met, which here is defined based on the relative error in the norm of residual forces as

$$\eta^{i+1} = \frac{\left\| \boldsymbol{\Psi}_n^{i+1} - \boldsymbol{\Psi}_n^{i} \right\|}{\|\mathbf{F}\|} \leq \eta^*, \tag{15}$$

with η^* being a preassigned target error, and $\mathbf{F} = \left\langle \mathbf{F}_{ext}, \tilde{\mathbf{F}}_{ext}^{\mathcal{HF}} - \mathcal{F}^{cohs} - \mathcal{F}^{\mathcal{HF}} \right\rangle^T$.

3.2 The fixed point algorithm

In practice, hydraulic fracturing treatments are generally performed through the application of constant injection rate at the borehole. In this fashion, pressure breakage and fluctuations—as crucial mechanisms in hydraulic fracturing—can be properly recognized (Milanese et al. 2016). Nevertheless, this set of boundary conditions (i.e., Eq. (10)) leads to an ill-posed singular set of equations regardless of the computational approach taken since the pressure field lacks a reference value (Nick and Matthäi 2011). It is noteworthy that in the literature, alternative boundary conditions can be found which circumvent this ill-posedness yet lack generality (e.g., through the assumption of the fracturing fluid pressure to be vanished at crack tips by Papanastasiou (1999), which is easily violated in toughness dominated propagation regimes (see Detournay 2004)).

To overcome the ill-posedness of the problem, following Boone and Ingraffea (1990) and Khoei et al. (2015), the injection rate at the borehole is replaced by the injection pressure as an *intermediate* boundary condition, which is modified such that the prescribed injection rate is acquired (i.e., $\left\{ (p|_{x'=0} \equiv p_{\mathcal{INJ}}) \Rightarrow (q|_{x'=0} \equiv q_{\mathcal{INJ}}) \right\}$). However, the imposition of such a boundary condition has been quite challenging, and the existing approaches in the literature suggest extremely inefficient algorithms which require a huge number of iterations (e.g., Boone and Ingraffea 1990; Secchi and Schrefler 2012; Khoei et al. 2015). Alternatively, here a super-convergent method is proposed which is claimed to ensure the satisfying convergence of the solution. Indeed the strong coupling between the two phases is responsible for the low convergence rate; yet, through the introduction of an indirect coupling scheme here the sources inducing oscillations in the solution are rapidly annihilated. To this end, the displacement field acquired

by the solution to the fractured bulk (i.e., Eq. 13) is replaced by a modified displacement field before being employed to solve the equations governing the hydro-fracture inflow (i.e., Eq. 14) as:

(i) *Scaling facture profile* A crucial source of failure in convergence is due to the fact that the pressure gradient is highly dependent upon the fracture profile (i.e., $\partial p/\partial x' \propto 1/h^3$). Even minor variations in fracture openings induce huge changes in the pressure field, which is a significant drawback in rapid convergence rate. To overcome this issue, the fracture profile is assumed to be self-similar within each iteration and is scaled to the target fracture volume by means of a scaling factor γ as

$$\bar{\mathbb{H}}^{i+1} = \gamma^{i+1}\mathbb{H}^{i+1}, \text{ where } \gamma^{i+1} = \left(\frac{\mathcal{V}^{\text{tar}}_{\mathcal{INJ}}}{(\mathcal{V}_{\mathcal{INJ}})^{i+1}}\right) \tag{16}$$

with $\mathcal{V}_{\mathcal{INJ}}$ and $\mathcal{V}^{\text{tar}}_{\mathcal{INJ}}$ being the current and target fracture volume, respectively (i.e., $\mathcal{V}_{\mathcal{INJ}} = \int_{x'=0}^{\ell_{\mathcal{HF}}} h\, dx$ and $\mathcal{V}^{\text{tar}}_{\mathcal{INJ}} = \mathcal{Q}_{\mathcal{INJ}}.t$).

(ii) *Implicit fracture profile* In staggered solutions, the fracture profile is observed to oscillate from one configuration to another within iterations. To circumvent such oscillations, the fracture profile is calculated implicitly by means of employing a weighted combination of the fracture openings in the previous two following iterations as

$$\bar{\bar{\mathbb{H}}}^{i+1} = \alpha\bar{\mathbb{H}}^{i+1} + (1-\alpha)\bar{\mathbb{H}}^{i}, \tag{17}$$

where α is the implicit weight factor ($0 \leq \alpha \leq 1$).

Using the abovementioned modification factors, the injection pressure is iteratively updated by using the modified fracture profile $\bar{\bar{\mathbb{H}}}^{i+1}$ as $p^{i+1}_{\mathcal{INJ}} = \lambda^{i+1} p^{i}_{\mathcal{INJ}}$, where λ is the pressure modification factor defined as $\lambda^{i+1} = (\mathcal{Q}^{\text{tar}}_{\mathcal{INJ}}/\mathcal{Q}^{i}_{\mathcal{INJ}})$. It is noteworthy that in Khoei et al. (2015) it is suggested to employ λ^{β} as the necessary and sufficient modification factor for the injection pressure with β being a reduction factor in range of $0 \leq \beta \leq 1.0$ (optimum at $\beta = 0.25$). In the numerical simulations section, the performance of the proposed approach is examined and compared to those existing in the literature.

4 Numerical simulation results

In this section, the performance of the proposed algorithm in the simulation of the hydro-fracture growth in semi-infinite domain is investigated. The first analytical solution to this example, known as the KGD problem, was proposed by Khristianovic and Zheltov (1955), and Geertsma and De Klerk (1969) and is in form of

$$\text{KGD}: \begin{cases} \text{CMOD} = c_1\left(\frac{\mu(1-\nu)\mathcal{Q}^3}{G}\right)^{1/6} t^{1/3} \equiv h|_{x'=0}\,, \\ \text{CL} = c_2\left(\frac{G\mathcal{Q}^3}{\mu(1-\nu)}\right)^{1/6} t^{2/3} \equiv \ell_{\mathcal{HF}}(t), \\ \text{CMP} = c_3\left(\frac{G^3\mathcal{Q}\mu}{(1-\nu)^3\ell^2_{\mathcal{HF}}}\right)^{1/4} + S \equiv p_{\mathcal{INJ}}(t), \end{cases} \tag{18}$$

where CMOD stands for the Crack Mouth Opening Displacement, CL is the Crack Length, and CMP is the Crack Mouth Pressure. In the above relations, c_i's are the model parameters, S is the in-situ stresses in direction normal to the fracture interface, ν is the Poisson's ratio, and G is the shear modulus. The KGD problem has been a classic benchmark in hydraulic fracturing research, which has been widely studied by using either the monolithic (Schrefler et al. 2006; Barani et al. 2011; Khoei et al. 2014) or the partitioned (Boone and Ingraffea 1990; Khoei et al. 2014, 2015; Nguyen et al. 2017) schemes. The material parameters employed here for the numerical analysis are: Young modulus of elasticity, $E = 15.96$ GPa; Poisson's ratio, $\nu = 0.2$; dynamic viscosity, $\mu = 1 \times 10^{-3}$ Pa.s; injection rate, $\mathcal{Q}_{\mathcal{INJ}} = 10^{-4}$ m^2/s; vapour pressure, $p_v \approx 0$MPa; ultimate tensile strength, $\sigma_{ult} = 1$ MPa; and Fracture toughness, $G_f \approx 0$ J/m^2. Notably, the cohesive fracture energy is assumed to be negligible so that the iterations are purely correlated with the nonlinearities induced by the partitioned coupling schemes. Using the more precise theoretical solution suggested by Spence and Sharp (1985), the model parameters are: $c_1 = 2.14$, $c_2 = 1.97$ and $c_3 = 0.65$. Unless specified otherwise, a FE mesh consisting of 2420 quadrilateral elements with 2448 nodal points is used for the numerical analysis. A schematic representation of the KGD problem is depicted in Fig. 2.

4.1 Partitioned solution strategies

In order to investigate the convergence rate of the partitioned schemes, three different solution strategies are considered here. Moreover, to examine the sensitivity of each solution algorithm to time increment,

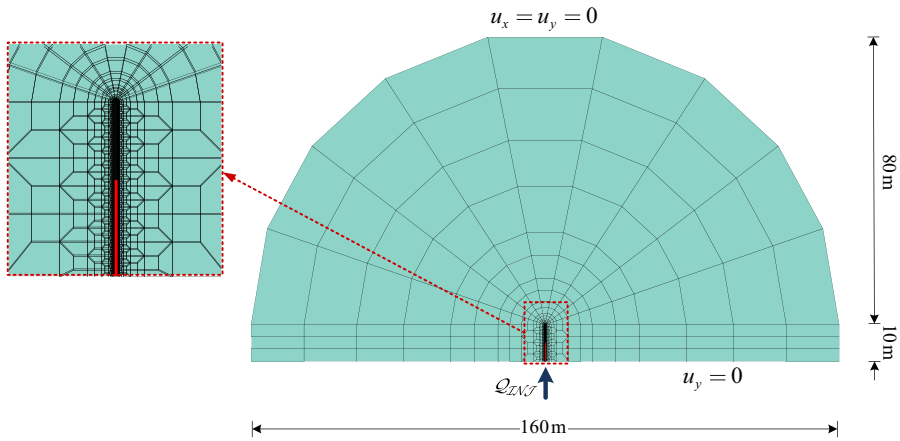

Fig. 2 Hydro-fracture growth in semi-infinite domain (the KGD problem); the problem definition, geometry and boundary conditions

all simulations are performed by using time increments of $\Delta t = 0.05$ and 0.2 s. Note that the relative error of $\eta^* = 10^{-6}$ is set as the convergence criterion for all the solutions here. In the first solution set, the proposed framework is employed in conjunction with the both modification factors of γ and α, where $\alpha = 0.0, 0.25, 0.5, 0.75, 1.0, (1.0 - i/i_{\max})$ and $i/i_{\max}$, with $i_{\max} = 100$. Note that in latter two cases (i.e., $(1.0 - i/i_{\max})$ and $i/i_{\max}$) α alters linearly from 1 to 0 or vice versa within the iterations. Moreover, the case of $\alpha = 0.0$ exercises no update to the hydro-fracture profile throughout the iterations, while in the case of $\alpha = 1.0$ the current deformation field is used explicitly. In the second solution set merely the weight factor α is applied in resemblance to the first solution set, yet the modifications due to the scaling parameter γ are disregarded (i.e., $\gamma = 1$). Finally, in the third solution set the existing staggered schemes in the literature–particularly the recent algorithm proposed by Khoei et al. (2015)–are examined in which the modification factor $\beta = 0, 0.25, 0.5, 0.75$ and 1.0 is utilized. It is noteworthy that the extreme case of $\beta = 0$ leads to no update in the injection pressure, while $\beta = 1.0$ yields the classic approach originally suggested by Boone and Ingraffea (1990).

In Fig. 3a–c, the variations of the CL, CMOD and CMP with respect to time are shown for the first solution set with $\Delta t = 0.05$s, and are compared to the analytical solutions by Spence and Sharp (1985). As can be seen, the proposed solution accords with the analytical solution in cases of $\alpha = 0.25, (1 - i/i_{\max}), i/i_{\max}$. In the rest of the cases substantial fluctuations occur which are eventually even further intensified with the evolution of the hydro-fracture in time. In Fig. 4a, the required number of the iterations for convergence is reported throughout all time steps of the solution. Note that wherever the number of iterations is reached at $i_{\max} = 100$, the algorithm has failed in convergence to the preassigned criterion (i.e., $\eta^* = 10^{-6}$). In Table 1, the average number of iterations $\bar{i}$, the variance σ^2 and the total number of iterations i_{total} is reported for all chosen weight factors. The case of $\alpha = 0$, despite showing the best convergence rate, suggests very inaccurate results. Indeed, the best result pertains to $\alpha = i/i_{\max}$ for involving the smallest average, the least total number of iterations, and more importantly the lowest variance. Thus, it can be concluded that the weight factor $\alpha = i/i_{\max}$ suggests the most robust, stable and reliable solution.

In Fig. 4b, the required number of iterations associated with the second solution set is reported. Evidently, for all the cases the maximum permitted number of iterations is exceeded, which indicates the failure in convergence. In this fashion, the necessity of the elaboration of the scale factor γ is shown. In Fig. 4c, the required number of iterations for the third solution set is provided. Despite increasing the upper limit for the permitted iterations to $i_{\max} = 200$, in no case is the convergence criterion met. This implies the very poor performance of the existing staggered algorithms in the literature. This accords with the requirement of thousands of iterations in the classic algorithms as reported by Boone and Ingraffea (1990). It is noteworthy that the time increment of $\Delta t = 0.05$s lies within the common range used in the numerical simulation of the KGD problem (e.g., see Schrefler et al. 2006; Barani et al. 2011; Khoei et al. 2014).

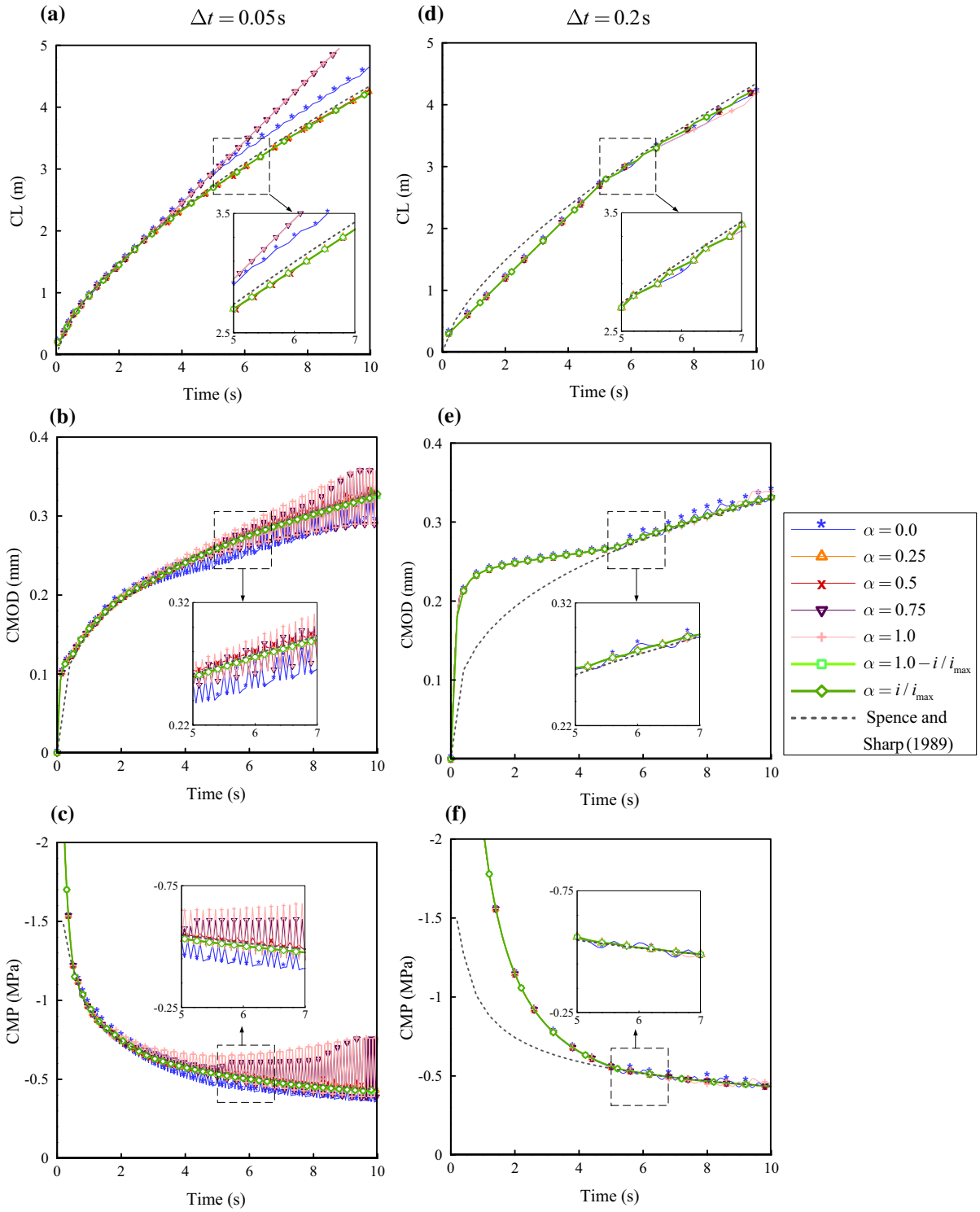

Fig. 3 The variations of Crack length (CL), Crack Mouth Opening Displacement (CMOD), and Crack Mouth Pressure (CMP) with time for $\Delta t = 0.05$s and $\Delta t = 0.2$s

Table 1 Number of iterations required for the convergence of the proposed method for different selections of α parameter

Δt(s)	α	$\bar{i}$	σ^2	i_{total}
0.05	0	10.61	3.255	2121
	0.25	30.32	825.2	6063
	0.5	51.37	1719.5	10,274
	0.75	50.01	1749.6	10,002
	1	54.84	1738.2	10,968
	$1 - i/i_{\max}$	67.86	756.41	13,572
	$i/i_{\max}$	23.77	38.881	4754
0.2	0	7.62	2.485	381
	0.25	13.5	5.316	675
	0.5	11.02	5.530	551
	0.75	23.38	610.53	1169
	1	49.68	1850.1	2484
	$1 - i/i_{\max}$	22.84	245.16	1142
	$i/i_{\max}$	23.46	27.723	1173

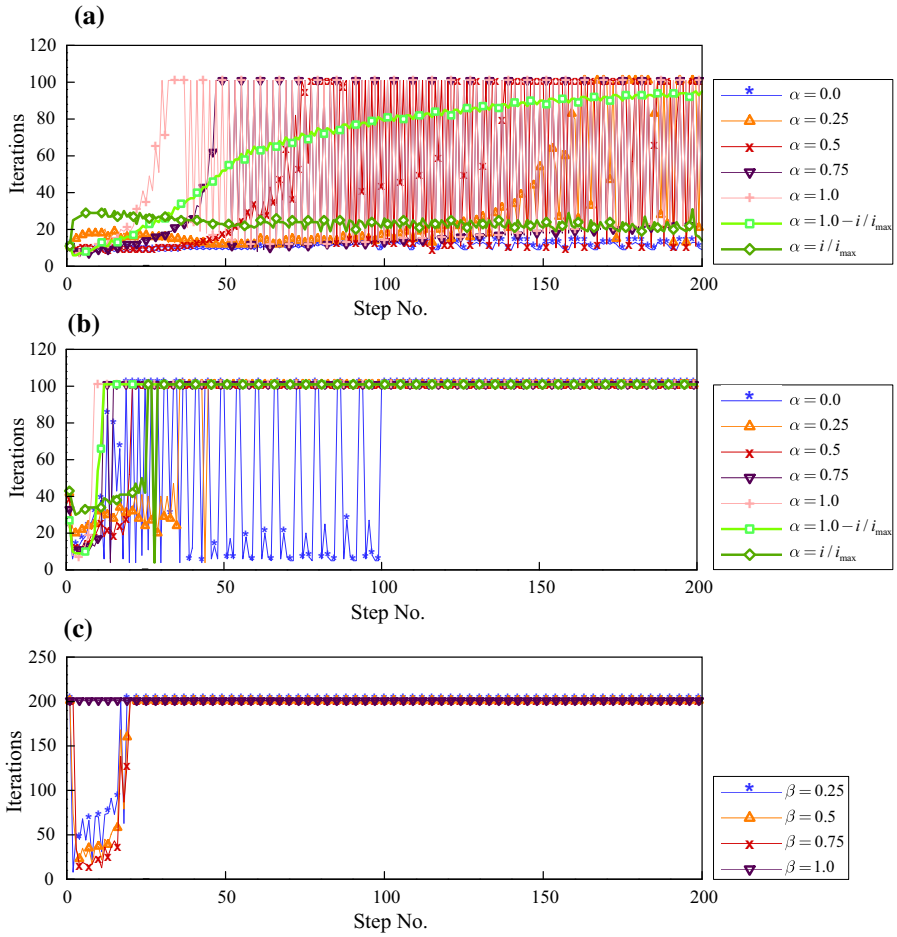

Fig. 4 Number of iterations required for convergence of $\Delta t = 0.05$s associated with: **a** proposed algorithm; **b** α-method; **c** β- method

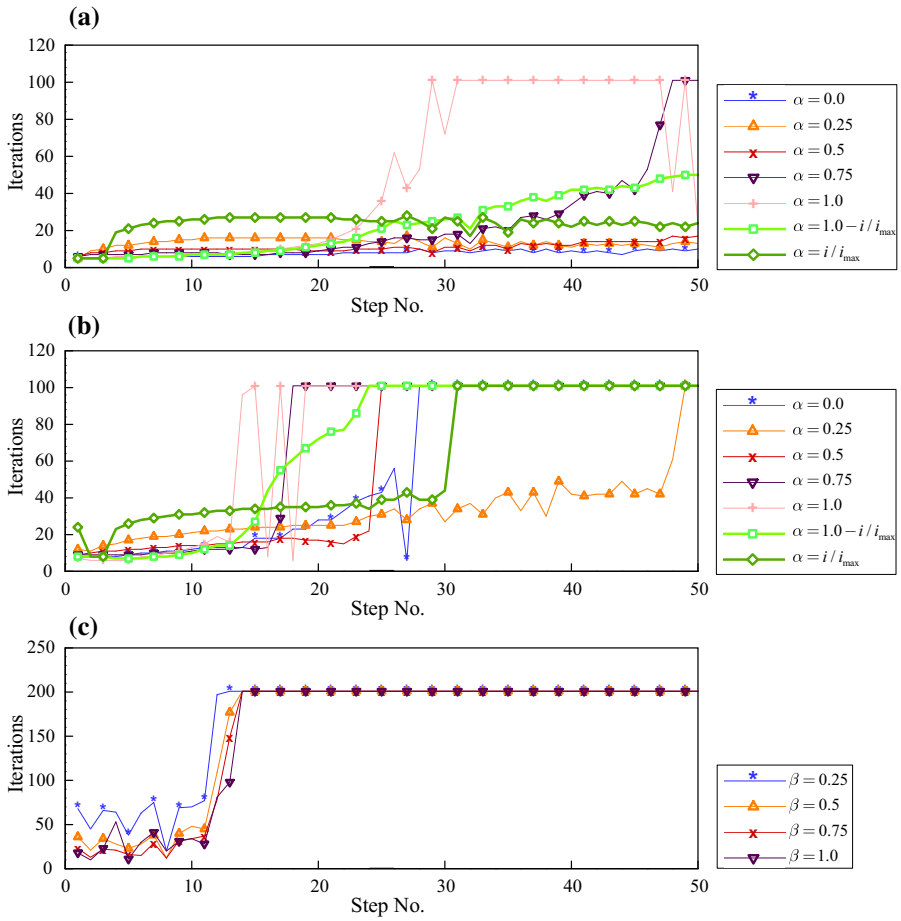

Fig. 5 Number of iterations required for convergence of $\Delta t = 0.2$s associated with: **a** proposed algorithm; **b** α-method; **c** β- method

The analysis is repeated for the time increment of $\Delta t = 0.2$s which is indeed very large for the current problem. In Fig. 3d–f, the variations of CL, CMOD and CMP with respect to time are reported for the first solution set. Except the extreme cases of $\alpha = 0.0, 1.0$ which show minor fluctuations, the rest of the cases behave quite smoothly. Notably, the discrepancies with respect to the analytical solution at the early stages are due to the elaboration of too large time increments for the analysis. In Fig. 5a, the required number of iterations associated with all the time steps of the solution is reported with the permitted number of iterations set to $i_{\max} = 100$. Evidently, excluding the case of $\alpha = 1.0$, all cases have now converged successfully within the allowable number of iterations. In Table 1, the statistical values associated with this solution set are also reported. As predicted, the case of $\alpha = 0$ represent the lowest values. Meanwhile, the case of $\alpha = i/i_{\max}$ stands to be the best solution regarding the simulation precision as well as with the statistical indexes. In Fig. 5b, the required number of iterations for the second solution set is presented. Clearly, substantial deterioration is observed in the convergence rate. This verifies the critical role of the proposed scaling factor, γ. Finally, in Fig. 5c the required number of iterations for the third solution set is depicted. Even though the time increment is enlarged significantly, a very poor convergence rate is observed for all the cases. More importantly, $\beta = 1$ generally shows the least required number of iterations which indicates the failure of this modification factor in improving the convergence rate.

At the end of this example, the required number of iterations associated with the third solution set for time increments of $\Delta t = 0.5$ and 1.0 s is demonstrated in Fig. 6. Evidently, the required number of iterations–now limited to $i_{\max} = 500$–shows a very poor performance. Notably, the best convergence rate is observed for $\beta = 1$, which is in fact the same as the classic solu-

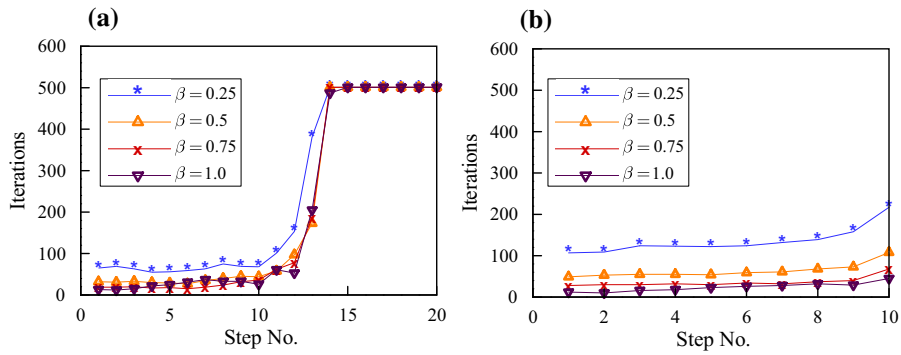

Fig. 6 Number of iterations required for convergence of β- method: **a** $\Delta t = 0.5$s; **b** $\Delta t = 1.0$s

tion suggested by Boone and Ingraffea (1990). Thus, the necessity of the modification factor β is dubitable. In this fashion, the crucial role of the proposed algorithm to the partitioned solution of the hydraulic fracturing problem is highlighted. Lastly, based on the simulations here, the existing staggered solutions are quite sensitive to the time increment; the required number of iterations significantly decreases by enlarging the time increments used for the simulation at the expense of reduction in accuracy.

4.2 Sensitivity analysis

In this example, the sensitivity of the proposed partitioned coupling scheme with respect to time increment as well as mesh size is investigated. To this end, three FE mesh consisting of 4643, 2420, 1545 quadrilateral elements in conjunction with 4683, 2448, 1570 nodal points, respectively, are applied which are referred to as the fine, medium and coarse mesh, respectively[1]. Notably, the majority of the elements are clustered in the vicinity of the hydro-fracture evolution trajectory, where the element sizes become as small as 12.5, 25 and 50 cm^2 in the fine, medium and coarse mesh, respectively. For each mesh refinement, a series of numerical analysis is performed using the time increments of $\Delta t = 0.025, 0.05, 0.1$ and 0.2 s. The relative error of $\eta^* = 10^{-6}$ is set as the convergence criterion in all cases. The modification factors of γ and $\alpha = i/i_{\max}$ are applied to provide the best convergence rate as suggested by the first example, with $i_{\max} = 100$.

In Fig. 7, the variation with time of the CL, CMOD and CMP is illustrated for all combinations of the mesh sizes and time increments. Again, the analytical solution by Spence and Sharp (1985) is included in all graphs as the reference solution. Evidently, the proposed solution strategy suggests promising results with improving trend as a result of either mesh refinement or reduced time increment. In Fig. 8, the required number of iterations throughout the time steps of the solution is reported for all mesh sizes and time increments. As can be seen, in all cases the convergence criterion is met within the permitted number of iterations with moderate fluctuations. In Table 2, the average, variance and total number of iterations is reported. Interestingly, in all cases the average number of required iterations is approximately the same (i.e., ~ 20). Meanwhile, the variance lies within very small ranges (i.e., $\sigma^2 \leq 50$). Such features are quite desirable from the computational perspective for being a representative of a robust and stable solution algorithm. Thus, in contrast to the existing staggered schemes in which the required number of iterations is too high, uncertain, and more importantly rapidly growing, the proposed scheme is quite promising.

Finally, the normalized error in the opening and fracturing pressure profiles with time, defined as $e_u = \|\mathbb{H} - \mathbb{H}_{\text{exact}}\| / \|\mathbb{H}_{\text{exact}}\|$ and $e_p = \|\mathbb{P} - \mathbb{P}_{\text{exact}}\| / \|\mathbb{P}_{\text{exact}}\|$, respectively, are shown in Fig. 9. To this end, the simulation results associated with the smallest time increment (i.e., $t = 0.025$s) are set as the exact solution. Notably, the comparisons are made at the final instant of the simulations (i.e., $t = 10$s). In this fashion, the convergence of the proposed framework with time is demonstrated.

5 Conclusions

In this paper, a super-convergent staggered Newton algorithm is proposed for the study of hydraulic fracturing problem. The momentum balance of the bulk,

[1] The medium mesh was formerly used in the first example.

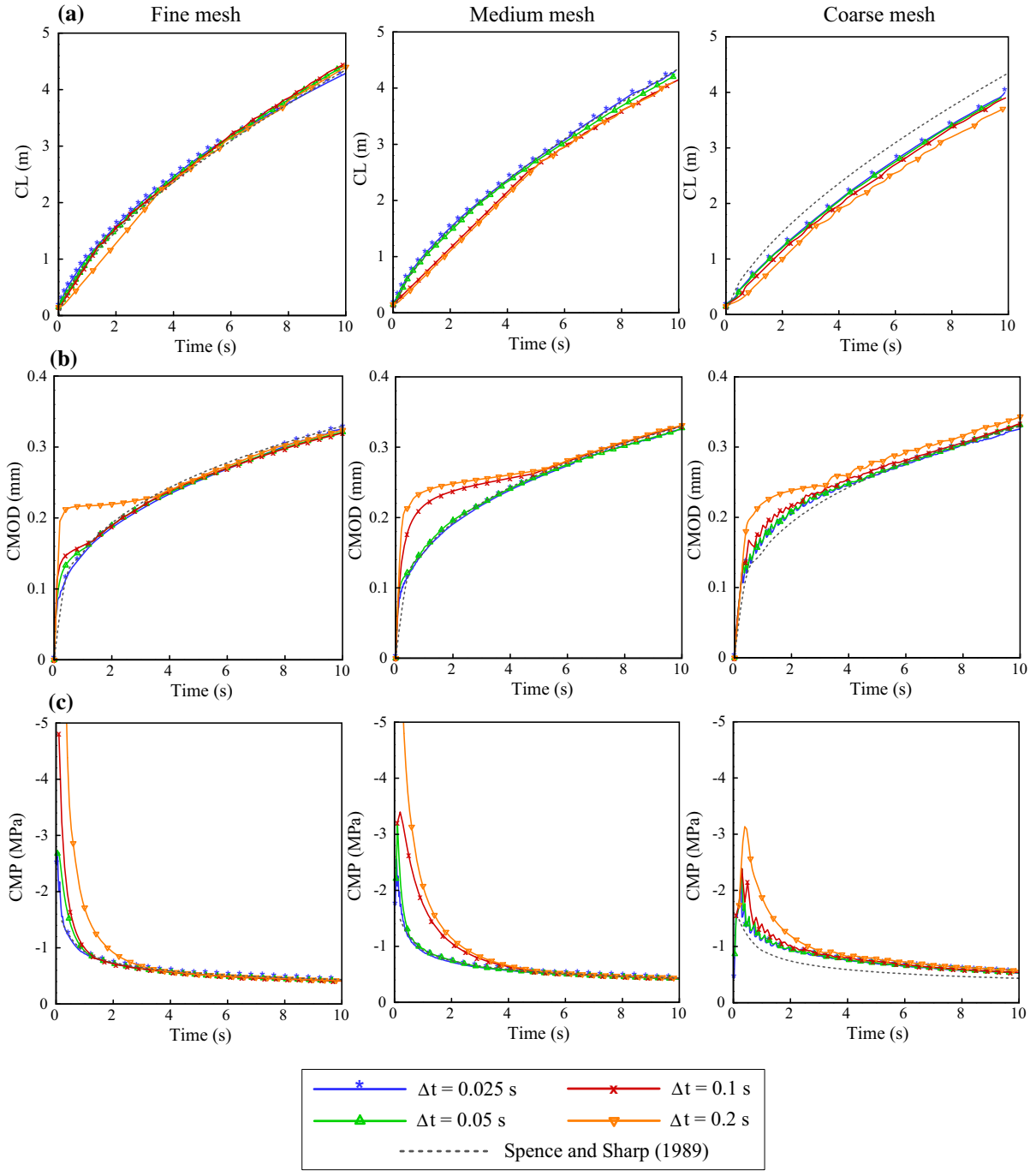

Fig. 7 The variations of Crack length (CL), Crack Mouth Opening Displacement (CMOD), and Crack Mouth Pressure (CMP) with time for the fine, medium, and coarse mesh

in conjunction with the flow continuity equations of the fracturing fluid flow forms the coupled system of the governing equations. A Newtonian viscous flow model is applied for the hydro-fracture inflow, where the fracture permeability is incorporated by using the cubic law. A staggered Newton algorithm is employed

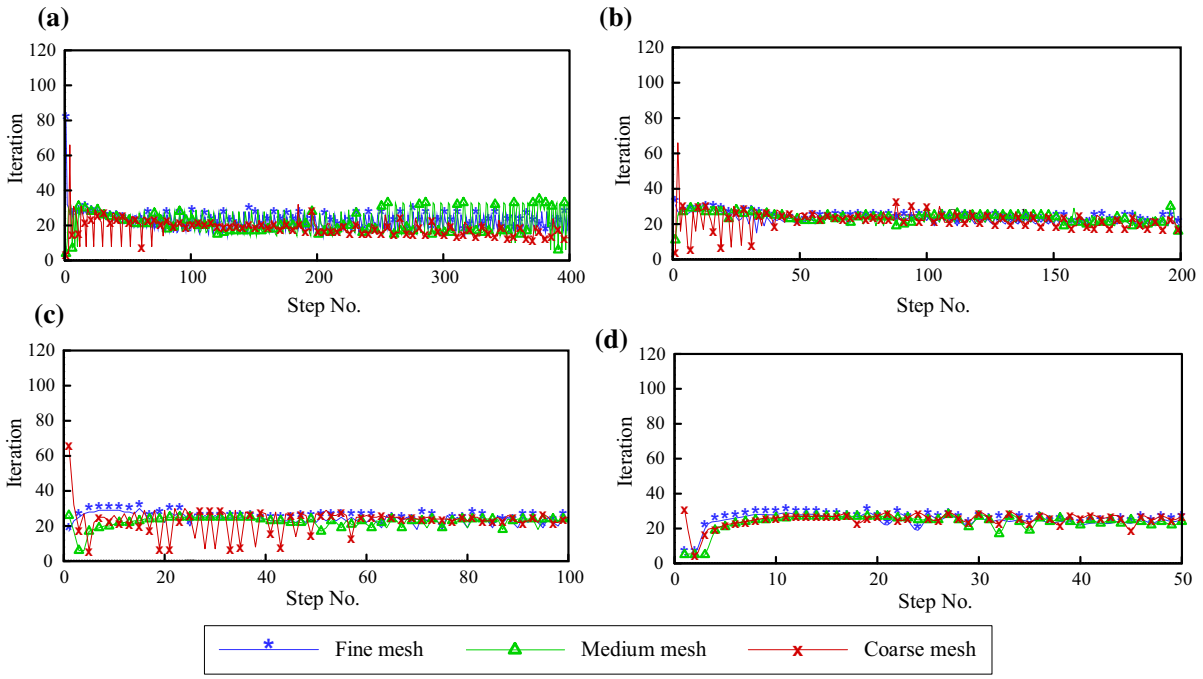

Fig. 8 Required number of iterations for convergence of the proposed algorithm for the fine, medium and coarse meshes; **a** $\Delta t = 0.025$s, **b** $\Delta t = 0.05$s, **c** $\Delta t = 0.1$s, and **d** $\Delta t = 0.2$s

Table 2 Number of iterations required for the convergence of the proposed method for a combination of mesh and time increment refinement

Δt(s)	Mesh size	$\bar{i}$	σ^2	i_{total}
0.025	Fine	21.98	23.528	8792
	Medium	22.20	44.339	8879
	Coarse	18.78	23.841	7512
0.05	Fine	22.70	5.349	4539
	Medium	23.77	38.881	4754
	Coarse	22.56	29.996	4512
0.1	Fine	24.14	7.314	2414
	Medium	22.38	10.440	2238
	Coarse	23.48	55.101	2348
0.2	Fine	24.26	20.727	1213
	Medium	23.46	27.723	1173
	Coarse	25.34	15.576	1267

to carry out the hydro-mechanical coupling. An innovative fixed-point algorithm is proposed which circumvents the difficulties encountered in the numerical convergence of the partitioned solution. In this regard, an indirect hydro-mechanical coupling scheme is introduced to minimize the issues which hinder the numerical convergence.

Through several sets of numerical simulation the robustness of the proposed framework is illustrated. In this regard, the convergence properties of the staggered solution to the well-known KGD problem are explored. In the first example, it is shown that the proposed framework–together with special combinations of the modification factors–suggests a smooth, stable and reli-

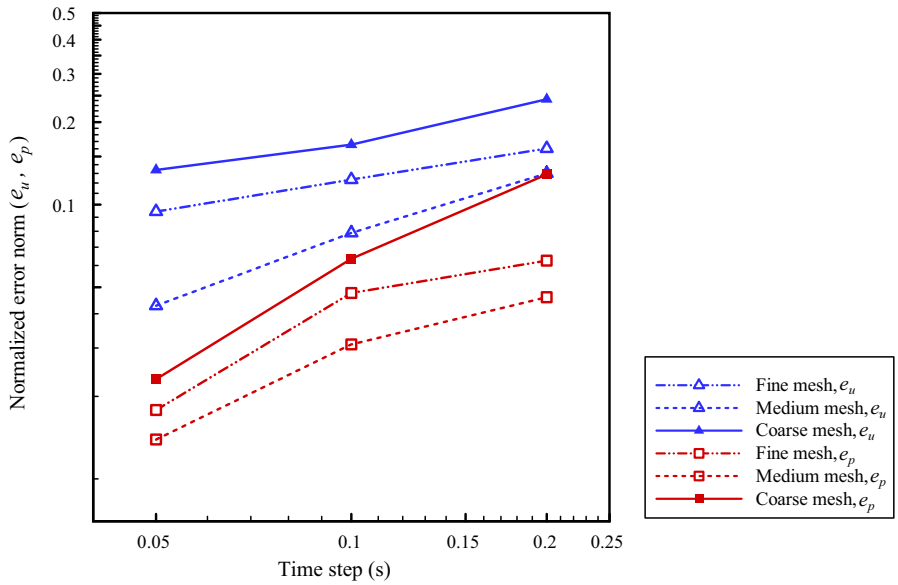

Fig. 9 Temporal convergence in aperture and pressure error norms for the hydro-fracture propagation in an impermeable domain; the average asymptotic rate of convergence is approximately 1.00 in the aperture error norm and 0.53 in the pressure error norm

able solution with excellent convergence rate. Meanwhile, the convergence rate of the existing staggered algorithms in the literature are examined and observed to behave poorly. Furthermore, as a major drawback, it is shown that by enlarging the time increment used for the simulations a better convergence rate is delivered. In the second example, through a comprehensive sensitivity analysis, it is shown that the proposed approach suggests a promising solution for a wide range of time increments as well as mesh refinements. In this fashion, the developed framework is deemed to be highly beneficial regarding the computational efficiency and accuracy of the partitioned solution to the hydraulic fracturing problem. The current framework can be extended to the study of multizone/multistage hydraulic fracturing treatments through the introduction of consistency constrains within the pressure field (see Haddad and Sepehrnoori 2016; Sheng et al. 2018; Sutula et al. 2018a, b, c), which is left to future studies.

Acknowledgements The authors wish to appreciate Professor Amir R Khoei (Sharif University of Technology), and Dr. Mohammad R Hirmand (University of Waterloo) for their valuable communications regarding the partitioned solutions.

References

Barani O, Khoei A, Mofid M (2011) Modeling of cohesive crack growth in partially saturated porous media; a study on the permeability of cohesive fracture. Int J Fract 167:15–31

Beach A (1980) Numerical models of hydraulic fracturing and the interpretation of syntectonic veins. J Struct Geol 2:425–438

Boone TJ, Ingraffea AR (1990) A numerical procedure for simulation of hydraulically-driven fracture propagation in poroelastic media. Int J Numer Anal Methods Geomech 14:27–47

Carter R (1957) Derivation of the general equation for estimating the extent of the fractured area. Appendix I of Optimum Fluid Characteristics for Fracture Extension, Drilling and Production Practice, GC Howard and CR Fast, New York, New York, USA, American Petroleum Institute, pp 261–269

Chen Y, Lian H, Liang W, Yang J, Nguyen VP, Bordas SP (2019) The influence of fracture geometry variation on non-Darcy flow in fractures under confining stresses. Int J Rock Mech Min Sci 113:59–71

Daneshy A (1978) Numerical solution of sand transport in hydraulic fracturing. J Pet Technol 30:132–140

Desroches J, Detournay E, Lenoach B, Papanastasiou P, Pearson J, Thiercelin M, Cheng A (1994) The crack tip region in hydraulic fracturing, Proceedings of the Royal Society of London A: Mathematical, Physical and Engineering Sciences. The Royal Society, pp 39-48

Detournay E (2004) Propagation regimes of fluid-driven fractures in impermeable rocks. Int J Geomech 4:35–45

Farhat C, Lesoinne M (2000) Two efficient staggered algorithms for the serial and parallel solution of three-dimensional nonlinear transient aeroelastic problems. Comput Methods Appl Mech Eng 182:499–515

Geertsma J, De Klerk F (1969) A rapid method of predicting width and extent of hydraulically induced fractures. J Pet Technol 21:1571–1581

Gordeliy E, Peirce A (2013) Coupling schemes for modeling hydraulic fracture propagation using the XFEM. Comput Methods Appl Mech Eng 253:305–322

Gordeliy E, Peirce A (2015) Enrichment strategies and convergence properties of the XFEM for hydraulic fracture problems. Comput Methods Appl Mech Eng 283:474–502

Haddad M, Sepehrnoori K (2016) XFEM-based CZM for the simulation of 3D multiple-cluster hydraulic fracturing in quasi-brittle shale formations. Rock Mech Rock Eng 49:4731–4748

Khoei AR, Hirmand M, Vahab M, Bazargan M (2015) An enriched FEM technique for modeling hydraulically-driven cohesive fracture propagation in impermeable media with frictional natural faults; Numerical and experimental investigations. Int J Numer Methods Eng 104:439–468

Khoei AR, Vahab M, Haghighat E, Moallemi S (2014) A mesh-independent finite element formulation for modeling crack growth in saturated porous media based on an enriched-FEM technique. Int J Fract 188:79–108

Khoei AR, Vahab M, Hirmand M (2016) Modeling the interaction between fluid-driven fracture and natural fault using an enriched-FEM technique. Int J Fract 197:1–24

Khoei AR, Vahab M, Hirmand M (2018) An enriched-FEM technique for numerical simulation of interacting discontinuities in naturally fractured porous media. Comput Methods Appl Mech Eng 331:197–231

Khristianovic SA, Zheltov YP (1955) Formation of vertical fractures by means of highly viscous liquid. In: 4th world petroleum congress. World Petroleum Congress

Lee S, Mikelić A, Wheeler MF, Wick T (2016) Phase-field modeling of proppant-filled fractures in a poroelastic medium. Comput Methods Appl Mech Eng 312:509–541

Lee S, Wheeler MF, Wick T (2017) Iterative coupling of flow, geomechanics and adaptive phase-field fracture including level-set crack width approaches. J Comput Appl Math 314:40–60

Lewis R, Schrefler B, Simoni L (1991) Coupling versus uncoupling in soil consolidation. Int J Numer Anal Methods Geomech 15:533–548

Matthies HG, Steindorf J (2003) Partitioned strong coupling algorithms for fluid-structure interaction. Comput Struct 81:805–812

Milanese E, Rizzato P, Pesavento F, Secchi S, Schrefler B (2016) An explanation for the intermittent crack tip advancement and pressure fluctuations in hydraulic fracturing. Hydraul Fract J 3:30–43

Mohammadnejad T, Khoei AR (2013) An extended finite element method for hydraulic fracture propagation in deformable porous media with the cohesive crack model. Finite Elem Methods Anal Des 73:77–95

Nguyen O, Repetto EA, Ortiz M, Radovitzky RA (2001) A cohesive model of fatigue crack growth. Int J Fract 110:351–369

Nguyen VP, Lian H, Rabczuk T, Bordas S (2017) Modelling hydraulic fractures in porous media using flow cohesive interface elements. Eng Geol 225:68–82

Nick H, Matthäi S (2011) Comparison of three FE-FV numerical schemes for single-and two-phase flow simulation of fractured porous media. Transp Porous Med 90:421–444

Papanastasiou P (1999) An efficient algorithm for propagating fluid-driven fractures. Comput Mech 24:258–267

Prevost JH (1997) Partitioned solution procedure for simultaneous integration of coupled-field problems. Commun Numer Meth En 13:239–247

Réthoré J, de Borst R, Abellan MA (2007) A two-scale approach for fluid flow in fractured porous media. Int J Numer Methods Eng 71:780–800

Samimi S, Pak A (2016) A fully coupled element-free Galerkin model for hydro-mechanical analysis of advancement of fluid-driven fractures in porous media. Int J Numer Anal Methods Geomech 40:2178–2206

Schrefler B, Simoni L, Turska E (1997) Standard staggered and staggered Newton schemes in thermo-hydro-mechanical problems. Comput Methods Appl Mech Eng 144:93–109

Schrefler B, Secchi S, Simoni L (2006) On adaptive refinement techniques in multi-field problems including cohesive fracture. Comput Methods Appl Mech Eng 195:444–461

Secchi S, Schrefler B (2012) A method for 3-D hydraulic fracturing simulation. Int J Fract 178:245–258

Segura J, Carol I (2008) Coupled HM analysis using zero-thickness interface elements with double nodes. Part I: Theoretical model. Int J Numer Anal Methods Geomech 32:2083–2101

Sheng M, Li G, Sutula D, Tian S, Bordas SP (2018) XFEM modeling of multistage hydraulic fracturing in anisotropic shale formations. J Petrol Sci Eng 162:801–812

Simoni L, Schrefler B (1991) A staggered finite-element solution for water and gas flow in deforming porous media. Int J Numer Method Biomed Eng 7:213–223

Simoni L, Schrefler BA (2014) Multi field simulation of fracture. In Advances in Applied Mechanics, Elsevier, pp 367–519

Saad Y (2003) Iterative methods for sparse linear systems (vol 82). SIAM

Spence D, Sharp P (1985) Self-similar solutions for elastohydrodynamic cavity flow. In: Proceedings of the royal society of London a: mathematical, physical and engineering sciences. The Royal Society, pp 289–313

Sutula D, Kerfriden P, Van Dam T, Bordas SP (2018a) Minimum energy multiple crack propagation. Part I: Theory and state of the art review. Eng Fract Mech 191:205–224

Sutula D, Kerfriden P, Van Dam T, Bordas SP (2018b) Minimum energy multiple crack propagation. Part-II: discrete solution with XFEM. Eng Fract Mech 191:225–256

Sutula D, Kerfriden P, Van Dam T, Bordas SP (2018c) Minimum energy multiple crack propagation. Part III: XFEM computer implementation and applications. Eng Fract Mech 191:257–276

Taleghani AD, Olson JE (2011) Numerical modeling of multistranded-hydraulic-fracture propagation: accounting for the interaction between induced and natural fractures. SPE J 16:575–581

Vahab M, Khalili N (2017) Numerical investigation of the flow regimes through hydraulic fractures using the X-FEM technique. Eng Fract Mech 169:146–162

Vahab M, Khalili N (2018) X-FEM modeling of multizone hydraulic fracturing treatments within saturated porous media. Rockmech Rock Eng 51:1–21

Wang J, Zhang Y, Liu J, Zhang B (2010) Numerical simulation of geofluid focusing and penetration due to hydraulic fracture. J Geochem Explor 106:211–218

Wells G, Sluys L (2001) A new method for modelling cohesive cracks using finite elements. Int J Numer Methods Eng 50:2667–2682

Wilson ZA, Landis CM (2016) Phase-field modeling of hydraulic fracture. J Mech Phys Solids 96:264–290

Witherspoon PA, Wang J, Iwai K, Gale J (1980) Validity of cubic law for fluid flow in a deformable rock fracture. Water Resour Res 16:1016–1024

Xia L, Yvonnet J, Ghabezloo S (2017) Phase field modeling of hydraulic fracturing with interfacial damage in highly heterogeneous fluid-saturated porous media. Eng Fract Mech 186:158–180

Zienkiewicz O, Chan A (1989) Coupled problems and their numerical solution, advances in computational nonlinear mechanics. Springer, Berlin, pp 139–176

Zienkiewicz O, Paul D, Chan A (1988) Unconditionally stable staggered solution procedure for soil-pore fluid interaction problems. Int J Numer Methods Eng 26:1039–1055